JOURNAL OF Materials CHEMISTRY

Synthesis and structure of microporous layered tin(IV) sulfide materials

Tong Jiang,[a] Alan Lough,[a] Geoffrey A. Ozin,*[a] Robert L. Bedard[b] and Robert Broach[b]

[a]*Materials Chemistry Research Group, Department of Chemistry, University of Toronto, Toronto, Ontario, Canada M5S 3H6*

[b]*UOP Research and Development, 50 E. Algonquin Rd., Des Plaines, Illinois 60017-5017, USA*

Synthetic methods have been developed which yield large single crystals and highly crystalline phase-pure microporous layered SnS-*n* materials. This allows study of the structure–property–function relations of these materials. The tin sulfide layer of the SnS-1 structure type contains hexagonally shaped 24-atom rings which are constituted by six Sn_3S_4 broken-cube cluster building units, linked together by double bridge $Sn(\mu\text{-}S)_2Sn$ sulfur bonds. The SnS-3 structure type contains elliptically shaped 32-atom rings which are also constructed from six Sn_3S_4 broken-cube clusters. However, they are linked by double bridge $Sn(\mu\text{-}S)_2Sn$ sulfur bonds as well as tetrahedral edge-bridging $Sn(\mu\text{-}S_2SnS_2)Sn$ spacer units. The SnS-1 structure type $[A_2Sn_3S_7]$ was obtained in the presence of $A^+ = Et_4N^+$, $DABCOH^+$ (protonated 1,8-diazabicyclooctane), and a mixed template system of NH_4^+/Et_4N^+, while the SnS-3 structure type $[A_2Sn_4S_9]$ emerged in the presence of $A^+ = Pr^n{}_4N^+$ and $Bu^n{}_4N^+$. Various SnS-1 and SnS-3 structures are examined and compared in relation to the size/shape of constituent template cations. A particular kind of structure-directing function was observed, that is, larger template molecules create larger void spaces within and between the tin sulfide sheets. Unique framework flexibility was discovered for both structure types. In order to accommodate the size/shape changes of templates, the flexible porous tin(IV) sulfide layers are able to undergo a certain degree of elastic deformation to alter the architecture of void spaces within and between the layers, rather than forming a completely new porous structure type. This is believed to be responsible for the relatively small number of structure types so far discovered for tin(IV) sulfide-based microporous layered materials compared to the myriad of three-dimensional open-framework structure types found for the zeolites and aluminophosphates. The observed differences among the various SnS-1 or SnS-3 structures is significant and has resulted in distinct adsorption behavior towards guest molecules. The TPA-SnS-3 framework is also found to be pressure sensitive. This all bodes well for envisaged chemical sensor applications for this class of porous materials.

Introduction

Microporous materials have been dominated by oxide-based structures, like zeolites, aluminophosphates and metal phosphates. Attributed to the uniform dimensions of void spaces in these materials, they have been widely used in selective catalysis, ion-exchange and as adsorbents.[1] The development of non-oxide-based microporous materials has received increasing attention in the last decade and many new material types have been synthesized and structurally characterized.[2] About a decade ago, Bedard and co-researchers at Universal Oil Products (UOP) patented novel families of microporous materials which were based on tin and germanium sulfide compositions.[3] These materials were synthesized under hydrothermal reaction conditions in the presence of an organic templating agent from SnS_2 and GeS_2 source materials. The metal sulfide-based microporous materials are of great academic and industrial interest. Given the semiconductor character of bulk tin and germanium sulfides, the microporous counterparts can be viewed as the geometric complement of semiconductor quantum dots, and have been envisaged to display distinct optical and electronic properties and quantum 'antidot' behavior.[4a,b] On the other hand, transition metal chalcogenides have been widely used as catalysts for hydrodesulfurization (HDS) processes of thiophene and related compounds. HDS catalysts made of microporous metal chalcogenides are anticipated to show enhanced selectivity, be less prone to poisoning, and display better overall performance. Microporous semiconductor materials may also find application in chemical sensing devices provided their electrical conductivity is sufficiently responsive and selective to the adsorption of different size/shape guest molecules.[4c]

In the original UOP patent, there was no structure information available on the tin sulfide-based microporous materials, denoted R-SnS-*n*, where R represents the occluded template cation and *n* the structure type. However, it was shown that TMA-SnS-1 displays a type 1 adsorption isotherm, that is characteristic of a microporous material. The products obtained from the synthetic method reported in the original patent generally feature small crystal size and contain impurity phases. Several SnS-*n* structures, *e.g.* TMA-SnS-1,[5] Cs-SnS-1,[6] TPA-SnS-3 and TBA-SnS-3,[7] have been solved since the publication of the original patent. However, there does not exist a detailed study and comparison of various structure types, nor an examination of the role of the template cations, nor a study of the effect of reaction conditions on the formation of the SnS-*n* materials. Although sufficiently large single crystals were obtained for structure determination in several cases, the samples often contained impurity phases. This complication inhibits the study of structure–property correlations for these materials.

Herein we describe details of the development of synthetic routes that yield large single crystals as well as phase-pure samples for some R-SnS-*n* phases. Structure determination is of course an essential prerequisite for the full characterization of solid state materials. While single crystal (SC) XRD structure analysis is preferable, sometimes the obtention of small crystals renders this practice impossible and then powder (P) XRD structure refinements become an invaluable aid. Phase-pure samples are desirable for the determination of the properties of materials. Knowledge gained through such studies enables the rational design and tailoring of structures and compositions with particular properties and functions. This report focuses attention on the synthesis and structure of two types of R-SnS-*n* materials, namely SnS-1 and SnS-3. The structure-directing role of the organic cations and the unique framework flexibility of these SnS-*n* materials will be presented. The effect

of the crystallization conditions on the formation of these SnS-*n* materials is examined. It should be mentioned that owing to their framework flexibility, the synthesis of a specific R-SnS-*n* material in both large single crystal and phase-pure forms turns out to be a very challenging task.

Synthesis of the R-SnS-*n* materials

Growth of large single crystals of R-SnS-*n* materials

Crystallization is believed to proceed through three basic steps: (i) dissolution of source materials in the presence of mineralizers, (ii) nucleation due to fluctuations in concentration and subsequent growth to viable nuclei, and (iii) growth of crystals.[8–10] In order to grow large single crystals of R-SnS-*n* materials, the three basic steps of crystallization have to be tuned to yield a small number of viable nuclei at the early stage of the crystallization process, so that each nucleus would have more of a supply of nutrients to feed its growth, and consequently evolve to a larger crystal size. Source materials and chemical reagents that affect their reactivity play an important role as they predetermine dissolution rates and the subsequent nucleation and crystal growth processes. An ideal source material would be one whose chemical reactivity is well known and can be readily controlled by a change of reaction conditions. Instead of using the source material SnS_2 as in the original patent, this work employed elemental tin, sulfur and sulfide as the source reagents for the hydrothermal synthesis of R-SnS-*n* materials. The vast literature on the chemistry of elemental Sn and S_8 has much to teach about their reactivity, *e.g.* their solubility, redox, surface and coordination chemistry. The redox chemistry and dissolution of Sn and S_8 can, to a large extent, be managed independently by altering concentration, pH, temperature profile, and agitation. More importantly, many coordination ligands or mineralizers can be used to control the rate of dissolution of Sn and S_8 in an aqueous environment. Details concerning the control of the crystallization conditions that favor the growth of large single crystals and phase-pure materials will be given in a separate paper where the mode of formation of the R-SnS-*n* materials is explored.[11]

In view of the well documented structure-directing role and templating function of organic molecules in the hydrothermal synthesis of microporous metal oxide materials, a range of organic amine and quaternary ammonium templates with different size and shape, Et_4N^+, $Pr^n{}_4N^+$, $Bu^n{}_4N^+$, DABCO (1,8-diazabicyclooctane), and a mixed template system of $NH_4{}^+$ and Et_4N^+ were employed in this study to explore their role in the formation of microporous metal sulfides. The different size of the template cations was expected to create porous materials with distinct porosity and framework architecture. The reaction mixtures and crystallization conditions that were optimised for the growth of large single crystals with these template systems are summarized in Table 1. The general practice is to seal the reaction mixture in a Teflon-lined stainless steel reactor and allow it to react and crystallize under static conditions with a predetermined temperature schedule. Single crystals of 100–500 μm in size were attained. Scanning electron micrograph (SEM) images of representative SnS-1 and SnS-3 crystals obtained in this way are displayed in Fig. 1.

Preparation of phase-pure R-SnS-*n* materials

Although large single crystals have been obtained from the static reactors described above, a considerable amount of metallic tin always remains unreacted at the end of crystallizations, in the form of small aggregate particles or disks. It is impossible to remove these from the product crystals without harming the products. The incomplete reaction of tin is believed to result from passivation processes that occur on the tin surface during the crystallization process. This suggests that agitation is required to obtain phase-pure products. A dynamic, end-to-end tumbling reactor was designed and constructed. Under dynamic conditions and appropriate reaction conditions the tin metal is expected to undergo complete dissolution. Another impurity that may co-form with the R-SnS-*n* materials is cassiterite, SnO_2. It is eliminated by the addition of excess sulfide into the initial reaction mixture, but retaining the molar ratio of elemental tin to sulfur at two in order to ensure complete redox reaction between the Sn and S elements. Table 2 summarizes the optimised conditions for the preparation of phase-pure SnS-1 and SnS-3 materials. In general, extended reaction times should be avoided as it tends to favor the formation of cassiterite impurity.

Structure characterization of the R-SnS-*n* materials

DABCOH-SnS-1

Single crystal refinement and crystallographic data of DABCOH-SnS-1 are summarized in Tables 3 and 4. The crystallographically defined formula for DABCOH-SnS-1 is $(DABCOH)_2Sn_3S_7{\cdot}H_2O$. As displayed in Fig. 2, DABCOH-SnS-1 features a microporous layered structure. The constituent tin(IV) sulfide anionic layer, $[Sn_3S_7]^{2-}$, is built up of Sn_3S_4 broken-cube clusters which are linked together by double bridge $Sn(\mu\text{-}S)_2Sn$ sulfur bonds to create pseudo-hexagonal-shaped 24-atom rings, Fig. 2A. (Note that, for the R-SnS-*n* materials this 24-atom ring notation refers to a pore constituted by 12Sn and 12S atoms, whereas in zeolite/molecular sieve materials, the jargon of the 24-atom ring refers to a pore based upon 24 tetrahedral T-atoms where T = Si, Al, P and 24O.) The cross-dimension of the pseudo-hexagonal pores is 10.983 Å × 10.983 Å × 9.95 Å as defined in Fig. 2A, measured from sulfur center to sulfur center. The free diameter of the pores is obtained by subtracting the van der Waals' diameter of sulfur from this value. The microporous tin(IV) sulfide sheet of DABCOH-SnS-1 is planar as in bulk SnS_2 with an interlayer spacing of 8.594 Å. It is interesting to note that the structure

Table 1 The optimised reaction mixture compositions and temperature profiles for the growth of large single crystals of the SnS-*n* materials

R-SnS-*n* material	composition of reaction mixture	crystallization conditions
$(NH_4)_{0.5}(Et_4N)_{1.5}Sn_3S_7$ (ATEA-SnS-1)	Sn : 1/4 S_8 : 2 $(NH_4)_2S$: TEAOH : 45 H_2O	heat to 150 °C in 24 h; hold at 150 °C for 24 h; cool to 20 °C in 12 h
$(Et_4N)_2Sn_3S_7$ (TEA-SnS-1)	Sn : 1/4 S_8 : TEAOH : 30 H_2O	heat to 150 °C in 2 h; hold at 150 °C for 72 h; cool to 20 °C in 40 h
$(DABCOH)_2Sn_3S_7$ (DABCOH-SnS-1)	0.2 DABCO : Sn : 1/4 S_8 : 2 $(NH_4)_2S$: 60 H_2O	heat to 150 °C in 12 h; hold at 150 °C for 30 h; cool to 20 °C in 20 h
$(Pr^n{}_4N)_2Sn_4S_9$ (TPA-SnS-3)	Sn : 1/4 S_8 : $Pr^n{}_4NOH$: NH_4F : 84 H_2O	heat to 150 °C in 2 h; hold at 150 °C for 72 h; cool to 20 °C in 20 h
$(Bu^n{}_4N)_2Sn_4S_9$ (TBA-SnS-3)	Sn : 1/4 S_8 : $Bu^n{}_4NOH$: 100 H_2O	heat to 150 °C in 2 h; hold at 150 °C for 72 h; cool to 20 °C in 20 h

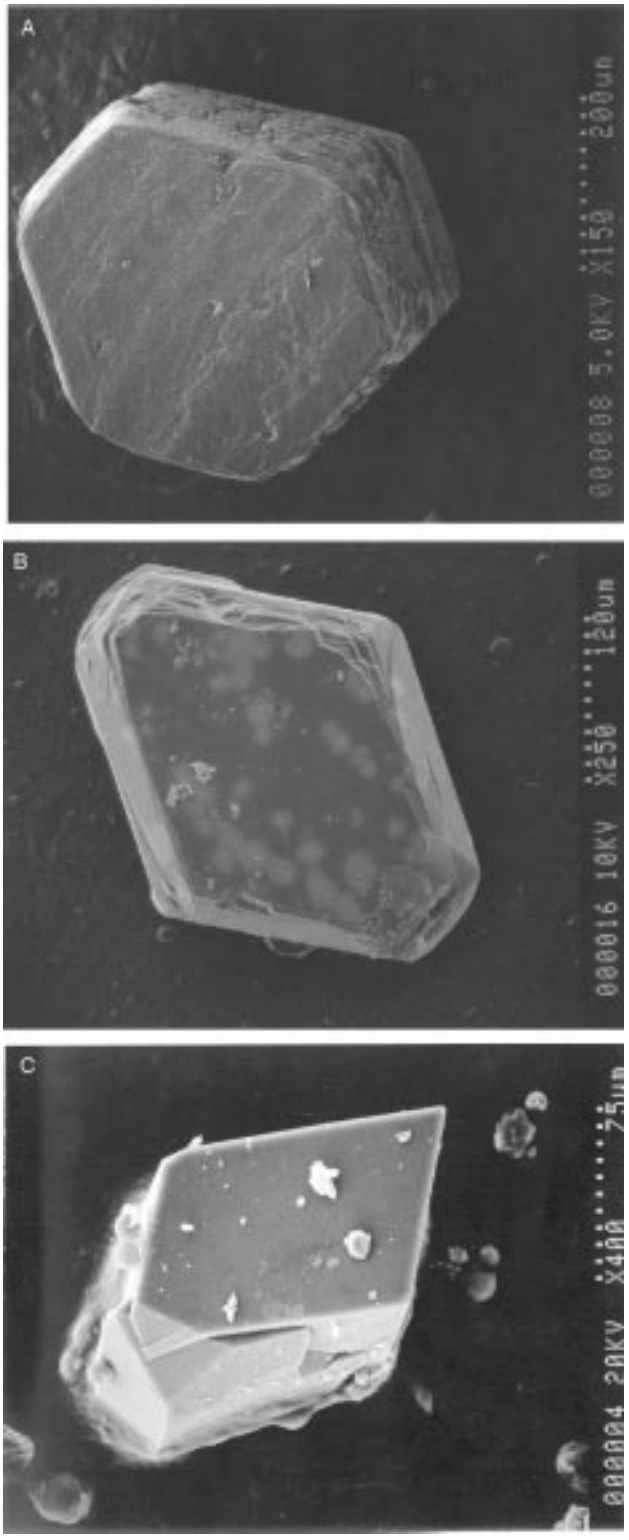

Fig. 1 SEM images of representative single crystals of (A) ATEA-SnS-1, (B) DABCOH-SnS-1 and (C) TPA-SnS-3

of bulk SnS_2 can also be viewed as being built-up of Sn_3S_4 broken-cube clusters; however, in SnS_2, these Sn_3S_4 clusters are linked together through edge-sharing Sn—S bonds to form close-packed tin sulfide layers. All of the tin(IV) atoms in the broken cubes of DABCOH-SnS-1 are five-coordinated with a pseudo-trigonal bipyramidal symmetry, while the sulfur(−II) is non-linear two- and trigonal pyramidal three-coordinated. The layer topology can be described as a 2,3-connected 2D net of trigonal pyramidal SnS_5 building units. In comparison, bulk SnS_2 contains only octahedral tin(IV) centers and trigonal pyramidal sulfur(−II). Bulk SnS_2 is a semiconductor with a calculated indirect optical band-gap of about 2.48 eV.[12] It is of great interest to see how the optical and electrical properties of bulk SnS_2 would be altered by the introduction of micropores within the tin sulfide layers. For example, are there any quantum size effects? Does the material behave as a quantum antidot lattice? Answers to these questions will be given in a separate paper.

The constituent layer, $[Sn_3S_7]^{2-}$, of the DABCOH-SnS-1 structure is negatively charged and the DABCO amine template is singly protonated, $DABCOH^+$, to counterbalance the charge. The proton from the $DABCOH^+$ cation is hydrogen bonded to the bridge sulfurs between the Sn_3S_4 broken-cube clusters (Fig. 2A) with nitrogen to sulfur distances of 3.218 and 3.305 Å, significantly shorter than 3.40 Å, the sum of the van der Waals' radii of S and N.[13] This indicates that negative charge on the tin(IV) sulfide layer is located around the bridging sulfurs between the Sn_3S_4 broken-cube clusters. This negative sulfur center is found to play a key role in the thermochemical behaviour of the DABCOH-SnS-1 material. It is interesting to note that the $DABCOH^+$ cations reside in the gap of the tin(IV) sulfide sheets in the DABCOH-SnS-1 structure, Fig. 2B. Two oxygen atoms are located inside the hexagonal-shaped 24-atom rings, with the shortest oxygen–sulfur distance of 3.719 Å, Fig. 2A. Presumably, these two oxygen atoms originate from occluded water molecules in the as-synthesized DABCOH-SnS-1 crystals. The relatively short oxygen–sulfur distance implies that the water molecules are weakly hydrogen bonded to the sulfur of the tin(IV) sulfide framework. It is found that these water molecules can be easily removed from the hexagonal rings, and well defined void spaces within the tin(IV) sulfide sheet can be generated. An interesting question is, would the dehydrated microporous layered DABCOH-SnS-1 behave like a molecular sieve? On the other hand, can the layered tin(IV) sulfide material also function as an intercalation host, *i.e.* swell the gaps between the tin sulfide sheets to incorporate guest molecules larger than the voids existing in the original structure?

The tin(IV) sulfide sheets in DABCOH-SnS-1 are stacked one on top of the other along the *c* crystallographic direction. One unit cell contains two tin(IV) sulfide sheets that are related by the *c* glide plane symmetry. The unit cell of DABCOH-SnS-1 has a space group of *C*2/*c*. The layer stacking sequence is thus described as AB type, for comparison with other SnS-1 structures. The pseudo-hexagonal shaped pores in these two tin(IV) sulfide sheets are slightly staggered and shifted by *ca.* 1/4 ***b*** unit along the *b* crystallographic axis, Fig. 2C. Elongated hexagonal channels, having a reduced dimension of *ca.* 1/2 ***b*** unit along the *b* axis, in comparison with the original 24-atom rings, can be viewed when looking down the *c* crystallographic axis.

ATEA-SnS-1

The single crystal refinement and crystallographic data of ATEA-SnS-1 are summarized in Tables 3 and 4. The crystallographically defined formula is $(NH_4)_{0.5}(Et_4N)_{1.5}Sn_3S_7{\cdot}H_2O$. As shown in Fig. 3A, ATEA-SnS-1 has a similar open layered structure to that of DABCOH-SnS-1. Its constituent tin(IV) sulfide anionic sheet, $[Sn_3S_7]^{2-}$, is also built up of Sn_3S_4 broken-cube clusters that are linked together in the same fashion as found in the DABCOH-SnS-1 structure. The charge-balancing NH_4^+ and Et_4N^+ cations mainly reside between the tin(IV) sulfide sheets. The difference between the constituent $[Sn_3S_7]^{2-}$ sheets in these two materials is that they display distinct symmetry and layer stacking sequences. ATEA-SnS-1 is crystallized in the space group $P3_121$, while DABCOH-SnS-1 in *C*2/*c*. One unit cell of ATEA-SnS-1 contains three parallel tin(IV) sulfide sheets that are related by the three-fold screw axis symmetry, Fig. 3B, C. The interlayer spacing is 9.011 Å. The Sn_3S_4 broken-cube clusters and hexagonal-shaped 24-

Table 2 The optimised reaction mixture compositions and temperature profiles for the synthesis of phase-pure SnS-*n* materials

R-SnS-*n* material	composition of reaction mixture	crystallization conditions
$(NH_4)_{0.5}(Et_4N)_{1.5}Sn_3S_7$ (ATEA-SnS-1)	Sn : 1/4 S_8 : $(NH_4)_2S$: TEAOH : 30 H_2O	tumbled, 150 °C for 1–2 days
$(Et_4N)_2Sn_3S_7$ (TEA-SnS-1)	Sn : 1/4 S_8 : TEAOH : 30 H_2O	static, 150 °C for 4 days, slow cooling to RT in 20 h
$(DABCOH)_2Sn_3S_7$ (DABCOH-SnS-1)	DABCO : Sn : 1/4 S_8 : $(NH_4)_2S$: 30 H_2O	tumbled, 150 °C for 1 day
$(Pr^n{}_4N)_2Sn_4S_9$ (TPA-SnS-3)	Sn : 1/4 S_8 : $Pr^n{}_4NOH$: 0.5 $(NH_4)_2S$: 160 H_2O	tumbled, 150 °C for 2–3 days

Table 3 Crystallographic data and structure refinement for DABCOH-SnS-1, ATEA-SnS-1 and TEA-SnS-1

	DABCOH-SnS-1	ATEA-SnS-1	TEA-SnS-1
empirical formula	$C_{12}H_{28}N_4OS_7Sn_3$	$C_{12}H_{32}N_2S_7Sn_3$	$C_{16}H_{40}N_2S_7Sn_3$
M_r	824.87	784.89	840.98
crystal size/mm	0.38 × 0.36 × 0.24	0.25 × 0.25 × 0.1	0.20 × 0.15 × 0.04
crystal class	monoclinic	hexagonal	monoclinic
space group	*C*2/*c*	$P3_121$	$P2_1/n$
temperature/K	173(2)	198(2)	294(2)
a/Å	22.281(9)	13.2560(2)	10.320(6)
b/Å	13.336(5)	13.2560(2)	13.340(3)
c/Å	17.188(7)	27.0336(7)	19.802(8)
β/°	105.53(1)	90	93.49(4)
V/A^3	4921(3)	4113.95(14)	2721(2)
Z	8	6	4
D_{calc}/g cm^{-3}	2.227	1.901	2.052
μ(Mo-K*α*)/cm^{-1}	36.3	32.45	32.8
F(000)	3184	2280	1648
ω scan width/°	0.46	0.80 + 0.35tan*θ*	0.80 + 0.35tan*θ*
range *θ* collected/°	2.67–30.21	1.77–28.27	2.1–48.0
independent reflections	6714	6657	3544
no. observed data	5802[$I > 2\sigma(I)$]	6657[R(int) = 0.0000]	2220[$I > 3\sigma(I)$]
refined on	F^2	F^2	F^2
R_1	0.0301[$I > 2\sigma(I)$]	0.0622	0.1657
wR_2, wR (all data)	0.0772	0.1412	0.2736
goodness-of-fit	1.009	1.119	1.90
parameters refined	254	123	123
maximum peak in final ΔF map/e $Å^{-3}$	0.826	1.685	5.36

Definition of *R* indices: $R_1 = \Sigma(F_o - F_c)/\Sigma(F_o)$, $wR_2 = \{\Sigma[w(F_o{}^2 - F_c{}^2)^2]/\Sigma[w(F_o{}^2)^2]\}^{1/2}$, $wR = \{\Sigma[w(F_o - F_c)^2]/\Sigma[w(F_o)^2]\}^{1/2}$.

atom rings in these three tin(IV) sulfide sheets are staggered by 120° when viewed orthogonally to the layers, Fig. 3B. Hexagonal-shaped channels can be viewed that are centered at the corners of unit cells and running down the *c* crystallographic axis. The layer stacking sequence in ATEA-SnS-1 is thus described as an ABC type, in comparison with the AB type in DABCOH-SnS-1. The 24-atom ring in ATEA-SnS-1 has an almost perfect hexagonal shape and its dimensions, as defined from sulfur center to sulfur center in Fig. 3A, are 10.935 Å × 10.935 Å × 10.878 Å. In contrast, the 24-atom rings of DABCOH-SnS-1 have an elongated hexagonal-shape with dimensions of 10.983 Å × 10.983 Å × 9.95 Å, Fig. 2A. The template cations, $NH_4{}^+$ and Et_4N^+, reside mainly between the gaps of the tin(IV) sulfide sheets. However, the ethyl groups are significantly extended into the 24-atom rings within the tin(IV) sulfide layer, Fig. 3C. This implies that the microsized pores within the layer are partially occupied by the Et_4N^+ cations. In contrast, in DABCOH-SnS-1 the template cations reside entirely within the gap between the tin(IV) sulfide sheets and the 24-atom rings are empty. One may wonder whether this would affect the adsorption properties of ATEA-SnS-1 in comparison with DABCOH-SnS-1. Would TEA-SnS-1 behave like a molecular sieve and/or an intercalation host?

TEA-SnS-1

TEA-SnS-1 also features a similar open 2D structure to those found in DABCOH-SnS-1 and ATEA-SnS-1, Fig. 4. It is crystallized in the $P2_1/n$ space group, different from both DABCOH-SnS-1 and ATEA-SnS-1 (Tables 3 and 4) but isostructural to TMA-SnS-1.[5] The single crystal data and structure refinement data of TEA-SnS-1 are summarized in Table 3. Note that although the final refinement of the TEA-SnS-1 structure is not as satisfactory as the other two structures, the unit cell and phase identity of TEA-SnS-1 were confirmed by powder XRD analysis as shown below.[14] The Raman and ^{119}Sn NMR spectra of TEA-SnS-1 also support the SnS-1 structure type of the TEA-SnS-1 material.[11b] The tin(IV) sulfide sheets are placed on the (2 0 2) Miller plane with an interlayer distance of 8.915 Å. The 24-atom ring is asymmetric as displayed in Fig. 4A. The unit cell of TEA-SnS-1 now contains only one tin(IV) sulfide sheet to give a stacking sequence of the AA type. The pseudo-hexagonal 24-atom rings from different layers are eclipsed and 24-atom rings channels of dimensions 11.58 Å × 10.84 Å × 10.42 Å can be observed when viewed down the *a* or *c* crystallographic axis.

Elemental analysis of TEA-SnS-1 suggests that the charge-balance of the anionic tin sulfide layer, $[Sn_3S_7]^{2-}$, is two Et_4N^+ cations. One of them was located by single crystal XRD analysis; it resides mainly between the gaps of the tin(IV) sulfide sheets. However, the ethyl groups are significantly extended into the 24-atom rings within the tin(IV) sulfide layer, Fig. 4B. Note that in the isostructural analog $(Me_4N)_2Sn_3S_7{\cdot}H_2O$ (TMA-SnS-1), as established through a single crystal analysis, both Me_4N^+ cations are entirely located

Table 4 (A) Atomic coordinates ($\times 10^4$) and equivalent isotropic displacement parameters (10^3 Å^3) for DABCOH-SnS-1 [U(eq) is defined as one third of the trace of the orthogonalized U_{ij} tensor

atom	x	y	z	U(eq)
Sn(1)	2909(1)	204(1)	−2369(1)	12(1)
Sn(2)	4227(1)	−1315(1)	−2413(1)	12(1)
Sn(3)	2783(1)	−2460(1)	−2502(1)	12(1)
S(1)	3119(1)	−1120(1)	−3382(1)	12(1)
S(2)	3884(1)	−2843(1)	−1938(1)	17(1)
S(3)	4011(1)	151(1)	−1704(1)	15(1)
S(4)	2309(1)	−1085(1)	−1939(1)	18(1)
S(5)	2715(1)	1488(1)	−1379(1)	15(1)
S(6)	2543(1)	1362(1)	−3437(1)	15(1)
S(7)	5324(1)	−1347(1)	−1467(1)	14(1)
N(1)	830(2)	830(3)	195(2)	24(1)
C(1)	501(2)	538(4)	631(3)	34(1)
C(2)	923(2)	653(4)	−1195(3)	35(1)
C(3)	1080(2)	1841(3)	177(3)	29(1)
C(4)	1582(2)	1845(3)	−273(3)	28(1)
C(5)	1349(2)	38(3)	499(3)	32(1)
C(6)	1762(2)	54(3)	−68(3)	27(1)
N(2)	1561(2)	861(3)	−688(2)	23(1)
N(3)	4274(2)	925(3)	−4256(2)	26(1)
C(7)	3608(2)	1003(3)	−4711(3)	32(1)
C(8)	3473(2)	2107(4)	−4891(3)	33(1)
C(9)	4377(2)	1416(4)	−3461(2)	30(1)
C(10)	4133(2)	2486(3)	−4722(2)	26(1)
C(12)	4528(2)	2527(3)	−4743(3)	29(1)
N(4)	3988(2)	2734(3)	−4449(2)	28(1)
O(1)	652(3)	1100(5)	1866(4)	106(2)

(B) Atomic coordinates ($\times 10^4$) and equivalent isotropic displacement parameters (10^3 Å^3) for ATEA-SnS-1 U(eq) is defined as one third of the trace of the orthogonalized U_{ij} tensor

atom	x	y	z	U(eq)
Sn(1)	7818(1)	4211(1)	8444(1)	24(1)
Sn(2)	10575(1)	4279(1)	8411(1)	24(1)
Sn(3)	7889(1)	1523(1)	8429(1)	24(1)
S(1)	8748(3)	3324(3)	7849(1)	25(1)
S(2)	9760(3)	5386(3)	8793(1)	29(1)
S(3)	6957(4)	5151(4)	8978(1)	34(1)
S(4)	6738(3)	2281(3)	8819(1)	30(1)
S(5)	9844(3)	2346(3)	8788(1)	30(1)
S(6)	7115(3)	4738(3)	7725(1)	29(1)
S(7)	7012(4)	−285(3)	8962(1)	31(1)
N(1)	4405(9)	1275(9)	7101(4)	31(2)
C(11)	5687(11)	1748(15)	7224(5)	42(3)
C(12)	3972(14)	399(12)	6674(5)	40(4)
C(13)	3690(14)	691(14)	7561(5)	45(4)
C(14)	4247(14)	2316(15)	6942(7)	47(4)
C(15)	6523(13)	2198(19)	6766(6)	58(5)
C(16)	4003(18)	1527(17)	7993(5)	55(5)
C(17)	4209(17)	−599(16)	6759(6)	55(5)
C(18)	3009(17)	2052(17)	6870(7)	62(5)
N(2)	10000	6716(14)	6667	42(4)
C(21)	9297(27)	5429(31)	6758(12)	41(10)
C(22)	9240(32)	7193(33)	6827(14)	63(14)
C(23)	10366(36)	7057(37)	6145(16)	97(19)
C(24)	11198(32)	7305(31)	6907(12)	56(12)
C(25)	10000	4731(20)	6667	73(10)
C(26)	10000	8651(39)	6667	146(28)
C(27)	10936(32)	7215(30)	7542(12)	140(18)
N(3)	8188(26)	8135(28)	9453(11)	164(11)

between the tin(IV) sulfide sheets with a lamellar spacing of 8.511 Å.[5] In view of the much larger diameter of Et_4N^+ compared with Me_4N^+, the relatively small increase of the interlamellar spacing to 8.915 Å in TEA-SnS-1 is consistent with the hydrocarbon arm of TEA being extended into the 24-atom ring space. This implies that the micropores within the layer are partially occupied by the Et_4N^+ cations. In comparison with ATEA-SnS-1 [$(NH_4)_{0.5}(Et_4N)_{1.5}Sn_3S_7$], TEA-SnS-1 [$(Et_4N)_2Sn_3S_7$] is expected to have smaller void spaces in the

Table 4 (*continued*) (C) Atomic coordinates ($\times 10^4$) and equivalent isotropic displacement parameters (10^3 Å^3) for TEA-SnS-1 [U(eq) is defined as one third of the trace of the orthogonalized U_{ij} tensor

atom	x	y	z	U(eq)
Sn(1)	0.0569(4)	0.9876(2)	0.4181(2)	0.022(1)
Sn(2)	0.1953(4)	1.1044(2)	0.2754(2)	0.026(1)
Sn(3)	0.1913(4)	0.8341(2)	0.2899(2)	0.024(1)
S(1)	0.2866(13)	0.9750(9)	0.3699(7)	0.026(5)
S(2)	0.0103(15)	1.1329(10)	0.3440(8)	0.036(5)
S(3)	0.1665(16)	0.9598(10)	0.1994(7)	0.030(5)
S(4)	0.0090(16)	0.8285(11)	0.3600(7)	0.038(5)
S(5)	0.3985(16)	1.1958(9)	0.2918(7)	0.032(5)
S(6)	0.1168(17)	1.2307(11)	0.1864(8)	0.043(6)
S(7)	0.1597(13)	1.0006(10)	0.5307(6)	0.025(4)
N(1)	0.6670(60)	0.9820(40)	0.1911(29)	0.057(15)
C(1)	0.5705(126)	0.9688(83)	0.1288(57)	0.114(37)
C(2)	0.4776(180)	1.0130(117)	0.1172(84)	0.159(64)
C(3)	0.5689(108)	0.9471(79)	0.2494(55)	0.112(34)
C(4)	0.6402(92)	0.9676(60)	0.3230(45)	0.083(26)
C(5)	0.8057(102)	0.8860(81)	0.2035(48)	0.107(32)
C(6)	0.7582(108)	0.7990(76)	0.1997(48)	0.101(30)
C(7)	0.7255(151)	1.0995(110)	0.1914(67)	0.168(51)

Table 5 A comparison of TPA-SnS-3 and TBA-SnS-3 structures

	TPA-SnS-3	TBA-SnS-3
formula	$(Pr^n{}_4N)_2Sn_4S_9$	$(Bu^n{}_4N)_2Sn_4S_9$
space group	$P2_1/n$	$Pbcn$
a/Å	15.513(3)	17.940(4)
b/Å	15.855(3)	19.498(4)
c/Å	18.627(4)	28.456(6)
β/°	110.43(3)	90
pore dimensions/Å[a]	20.65 × 9.32	19.8 × 11.3
interlamellar dimension/Å	14.05	14.2
layer stacking sequence	AA	ABAB

[a]Dimensions defined as sulfur center to sulfur center (see Fig. 6).

24-atom rings, as it has only Et_4N^+ cations as template, however, with a slightly smaller interlamellar spacing than ATEA-SnS-1.

TPA-SnS-3

A new structure type, SnS-3, is formed when tetrapropylammonium is employed as the templating agent. The single crystal XRD structure data for TPA-SnS-3 have been published earlier and the crystallographic details deposited in the Cambridge database.[7] The unit cell parameters of TPA-SnS-3 are listed in Table 5. The crystallographically defined formula for TPA-SnS-3 is $(Pr^n{}_4N)_2Sn_4S_9$. Like the SnS-1 materials described above, TPA-SnS-3 also features an open layered structure that is built up of the Sn_3S_4 broken-cube clusters, Fig. 5A. However, these Sn_3S_4 clusters are interconnected by tetrahedral edge-bridging Sn(μ-S_2SnS_2)Sn spacer units as well as double bridge Sn(μ-S)$_2$Sn sulfur bonds, to generate the elliptically shaped 32-atom rings, Fig. 5A. In addition, the constituent tin(IV) sulfide sheets, $[Sn_4S_9]^{2-}$, have developed a unique kind of curvature to result in a parallel stacked, corrugated layer structure in TPA-SnS-3, Fig. 5B. The tin(IV) sulfide sheet of TPA-SnS-3 can also be viewed in terms of a staircase, having holes that completely fill the horizontal and vertical parts of each step. When viewed perpendicularly to the steps of these corrugations, quasi-rectangular shaped pores are revealed, Fig. 5D. The angle between the vertical and horizontal components constituting the steps in the corrugated layer is about 88°. The layer stacking sequence in TPA-SnS-3 may be described as AA type as there is only one tin(IV) sulfide layer in the unit cell. The charge-balancing cations, $Pr^n{}_4N^+$, reside in the void space within and between the microporous tin(IV) sulfide layers, Fig. 5C,B. TPA-SnS-3 contains both five-coordinate pseudo-trigonal bipyramidal SnS_5 and four-coordinate pseudo-tetra-

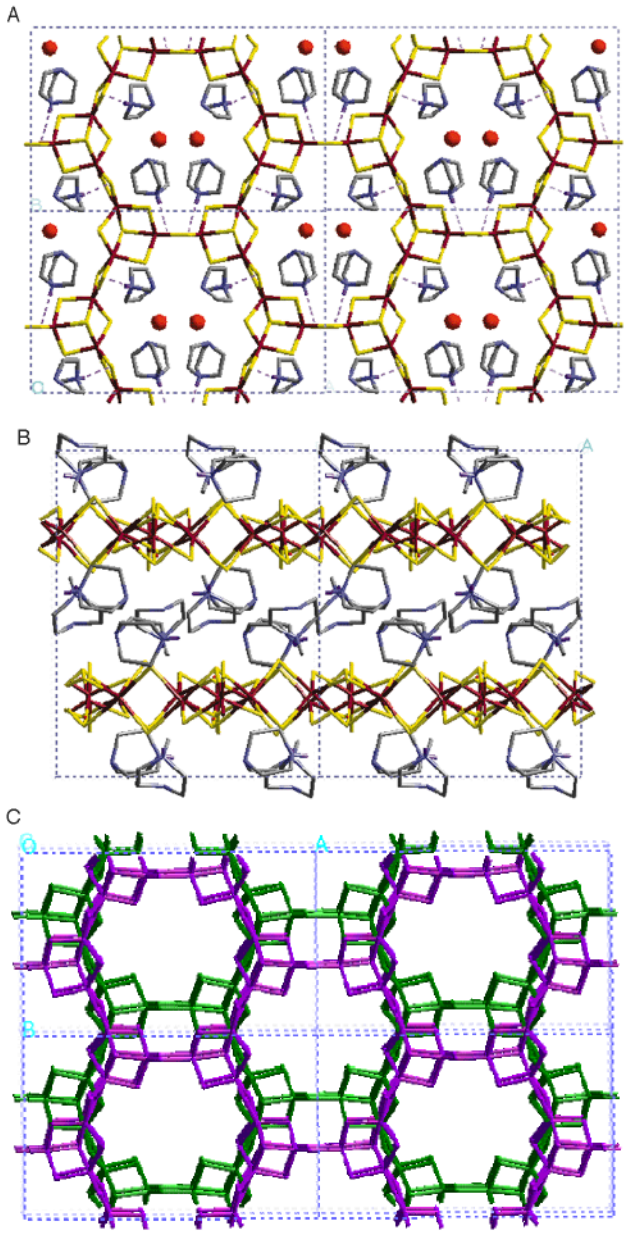

Fig. 2 An illustration of the 2D porous structure of DABCOH-SnS-1 (color notation: dark red, Sn; yellow, S; blue, N; grey, C; purple, H; red, O). Projection of (A) the [001] plane; (B) [100] plane, showing the $DABCOH^+$ cations located between the tin sulfide sheets and (C) [001] plane, showing the two tin(IV) sulfide layers within one unit cell offset by *ca.* 1/4 ***b*** unit along the *b* axis, and hexagonal-shaped channels running down the *c* axis with dimensions smaller than the 24-atom rings by *ca.* 1/4 ***b***.

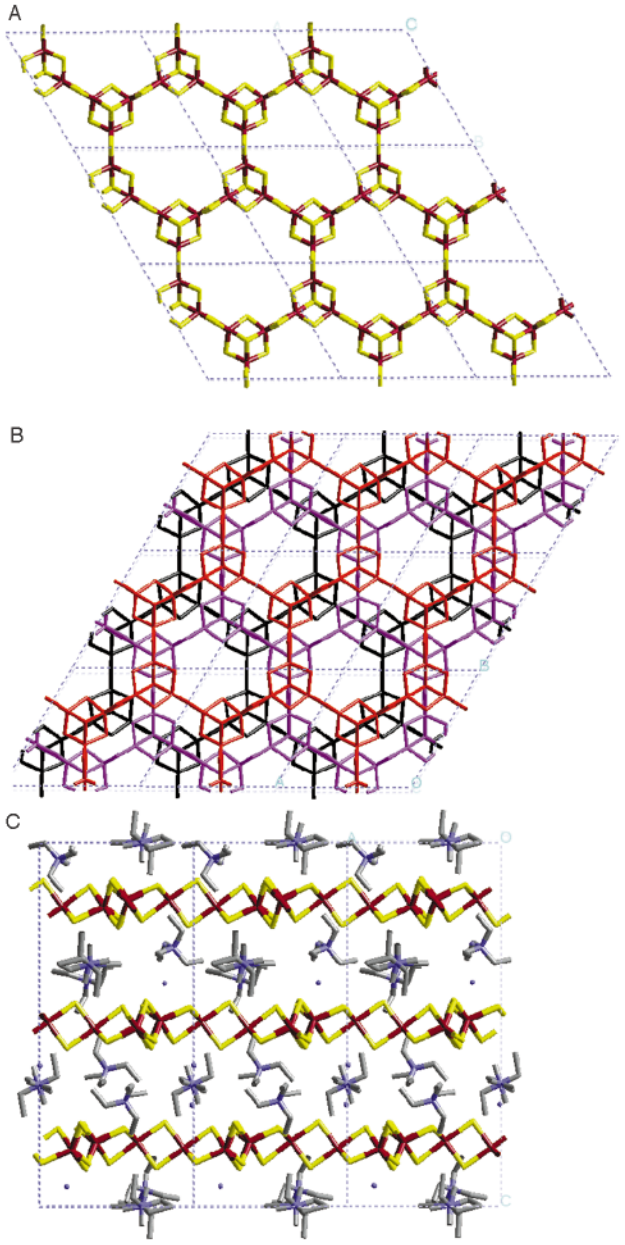

Fig. 3 Illustrations of the structure of ATEA-SnS-1 (color notation: dark red, Sn; yellow, S; blue, N; grey, C). (A) Projection of the [001] plane with the NH_4^+ and Et_4N^+ cations omitted for clarity, showing a single $[Sn_3S_7]^{2-}$ tin(IV) sulfide layer with hexagonal-shaped 24-atom rings, (B) projection of the [001] plane, showing that there are three tin(IV) sulfide layers in one unit cell that are connected by the 3_1 screw axis and (C) projection of the [010] plane showing the Et_4N^+ cations extended into 24-atom rings within the tin sulfide layer (note that one of the Et_4N^+ is distorted).

hedral SnS_4 units. The sulfur(−II) is two- and three-coordinated as in the SnS-1 structure.

TBA-SnS-3 is formed when tetrabutylammonium is used as the template cation. The structure of TBA-SnS-3 is found to resemble that of TPA-SnS-3.[7] It also features a porous layered structure with a composition of $[Sn_4S_9]^{2-}$ for the tin(IV) sulfide constituent layer, Fig. 6. The unit cell parameters of TBA-SnS-3 are shown in Table 5. TBA-SnS-3 has a distinct space group *Pbcn*, in comparison with TPA-SnS-3 which has a space group of $P2_1/n$. As a result, the tin(IV) sulfide porous layers of TPA-SnS-3 and TBA-SnS-3 display a different symmetry and layer stacking sequence, similar to what has been observed for the different SnS-1 materials. The 32 atom-ring elliptical-shaped pores are regular in TBA-SnS-3 and distorted in TPA-SnS-3, Fig. 6,5A. A comparison of the pore size and shape and interlamellar spacings between these two R-SnS-3 materials is summarized in Table 5. The layer stacking in TBA-SnS-3 is described as AB type with two parallel tin(IV) sulfide sheets in one unit cell.

Discussion

Templating effect of the organic cations

The role of organic cations in hydrothermal synthesis is generally recognized as structure-directing, charge-balancing and void-filling. Templating agents with different shapes and sizes have been successfully used to produce a large variety of open-framework materials. Small simple organic molecules have resulted in many microporous materials with pore dimensions up to almost 20 Å.[15] 'Supramolecular templating' using liquid crystals and micelles has enabled the generation of novel mesoporous materials with pore dimensions between 20 and

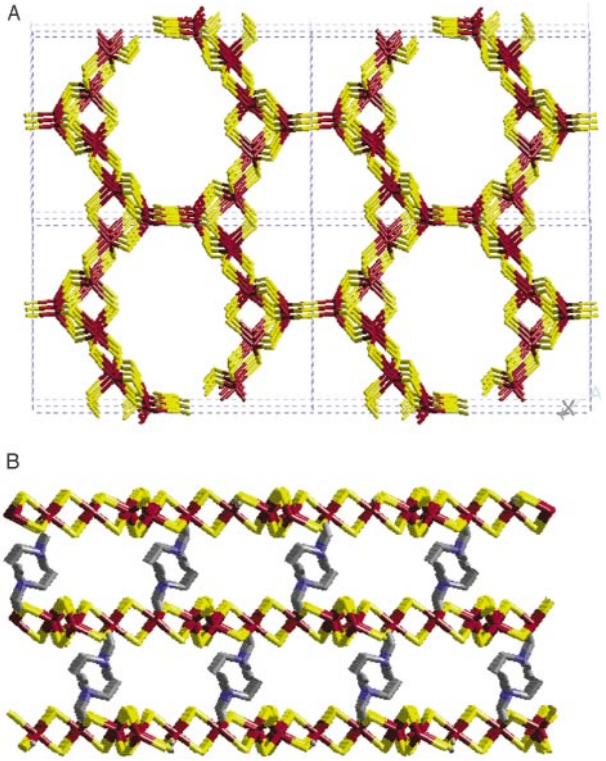

Fig. 4 Illustrations of the structure of TEA-SnS-1 (color notation: dark red, Sn; yellow, S; blue, N; grey, C). (A) Projection of the [101] plane with Et_4N^+ cations omitted for clarity, showing $[Sn_3S_7]^{2-}$ tin(IV) sulfide layers with distorted hexagonal-shaped 24-atom rings and hexagonal-shaped channels, (B) projection of the [010] plane showing the Et_4N^+ cations extended into the 24-atom rings within the tin sulfide layer.

100 Å.[16] The cooperative organization of organic–inorganic assemblies is believed to play a key role in the formation mechanism of these porous materials.

In the assembly of the SnS-*n* materials, the organic cations also appear to have a particular kind of templating function. The 24-atom rings present in the SnS-1 structure is templated by smaller cations, $DABCOH^+$, NH_4^+/Et_4N^+ and Et_4N^+, while the larger cations, $Pr^n{}_4N^+$ and $Bu^n{}_4N^+$, have led to the 32-atom rings present in the SnS-3 structure. The interlamellar spacing is about 8.5–9 Å in the SnS-1 structure, and about 14 Å in the SnS-3 structure. The SnS-1 structure type has also been templated by trimethylammonium[17] and tetramethylammonium[5] cations. The pore size and interlamellar spacing among the various SnS-1 materials also display certain correspondence with the size of the template cations as summarized in Table 6. Interestingly, the Cs^+ cation with a diameter of 1.81 Å[13] has templated an open-layered structure, $Cs_4Sn_5S_{12}$, in which 20-atom rings are present in the tin(IV) sulfide layer with an interlamellar spacing of 7.166 Å.[18] However, in the presence of cyclooctasulfur molecules, Cs-SnS-1 ($Cs_2Sn_3S_7{\cdot}0.5S_8$) has been synthesized.[6] Cs-SnS-1 is isostructural with $(DABCOH)_2Sn_3S_7{\cdot}H_2O$. The Cs^+ cations are located between the tin sulfide gaps to give an interlamellar distance of 8.151 Å. The 24-atom rings are occupied by cyclooctasulfur rings which cannot be removed without harming the integrity of the tin sulfide framework. It appears that the cyclooctasulfur molecule functions as a co-templating agent with the Cs^+ cation, and the Cs^+ alone may not be large enough to direct the formation of SnS-1 structure.

Framework flexibility of the R-SnS-*n* materials

Template induced framework flexibility

The remarkable structural differences among the R-SnS-1 and R-SnS-3 families of materials indicate that the bonding between tin and sulfur, and thus the constituent $[Sn_3S_7]^{2-}$ and $[Sn_4S_9]^{2-}$ tin(IV) sulfide layers, is extremely flexible. As summarized in Tables 5 and 6, the shape and size of the 24-atom rings in SnS-1 and the 32-atom rings in SnS-3 structures, as well as the layer stacking sequence and interlamellar spacings, can be modified considerably in response to the change of size and shape of the organic templates. This phenomenon may explain the relatively smaller structural variety so far observed for microporous tin(IV) sulfide-based materials in comparison with the myriad of structure types for the oxide-based microporous relatives like zeolites and aluminophosphates. In order to accommodate the size/shape changes of templates, the microporous layers of the tin(IV) sulfide materials undergo elastic deformation to alter the void spaces within and between the layers, rather than forming a completely new microporous structure type. This is to be contrasted with 3D microporous structures, in which there exists a greater restriction on the size and shape of the void space, either a cavity or channel, which can hardly be modified without an accompanying complete reorganization of the 3D framework. However, it should be mentioned that the open frameworks of RHO and ZSM-5 zeolite materials have been found to display interesting framework flexibility but of a different type to that described for the SnS-*n* materials.[19] It has also been shown that a similar structural flexibility of the R-SnS-*n* structures can be induced by adsorbed guest molecules with a concomitant change in optical and electrical properties.[20] The unique structural flexibility of these materials makes them of considerable interest as potential chemoselective sensory elements for molecular recognition devices.[4c,20c]

It is interesting to note that the framework flexibility of the SnS-*n* materials is related to the well known polytype phenomenon occurring in bulk SnS_2. They all originate from the flexible bonding nature of tin(IV) and sulfur(−II) centers. However, the constituent tin sulfide layer in different SnS_2 polytypes is identical and all of the polytypes have the same 2D unit cell parameters and structure within the tin sulfide sheet. The only difference among them is the stacking sequence of the constituent layers and the cell parameter along the stacking direction.[21] In this regard, different SnS-1 or SnS-3 structures have distinct 3D cell parameters and space groups and are better regarded as polymorphs.[21] Furthermore, the tin sulfide constituent layer in each particular structure has unique Sn−S bond angles and distances, and therefore a distinct pore size and shape. It appears that the tin–sulfide trigonal bipyramidal and tetrahedral connecting units that create the regular microscopic perforations of the tin sulfide layer, can act as flexible hinge-points to give pliability to the tin sulfide-based layered structures.

Pressure induced flexibility

The R-SnS-*n* materials are found to be pressure sensitive. For example, TPA-SnS-3, when ground in a mortar with moderate grinding force, readily transforms to a new phase, denoted TPA-SnS-3(II), as detected by PXRD, Fig. 7. TPA-SnS-3(II) has a slightly reduced interlamellar spacing of 9.85 Å, in comparison with that of the original TPA-SnS-3 phase, 10.42 Å. The smaller number of diffraction lines diagnostic of the TPA-SnS-3(II) phase implies that it has a higher symmetry. Justification for calling this phase SnS-3 stems from the similarity of the ^{119}Sn CP MAS NMR spectra of the original TPA-SnS-3 and TPA-SnS-3(II).[11b] It is interesting to mention that the discovery of the pressure sensitivity of TPA-SnS-3 was rather interesting. As described earlier, different synthetic routes had to be developed for the synthesis of large single crystals as distinct to phase-pure powders of the SnS-*n* materials. After the successful determination of the TPA-SnS-3 structure by SCXRD analysis, considerable synthetic effort was devoted to the preparation of phase-pure TPA-SnS-3

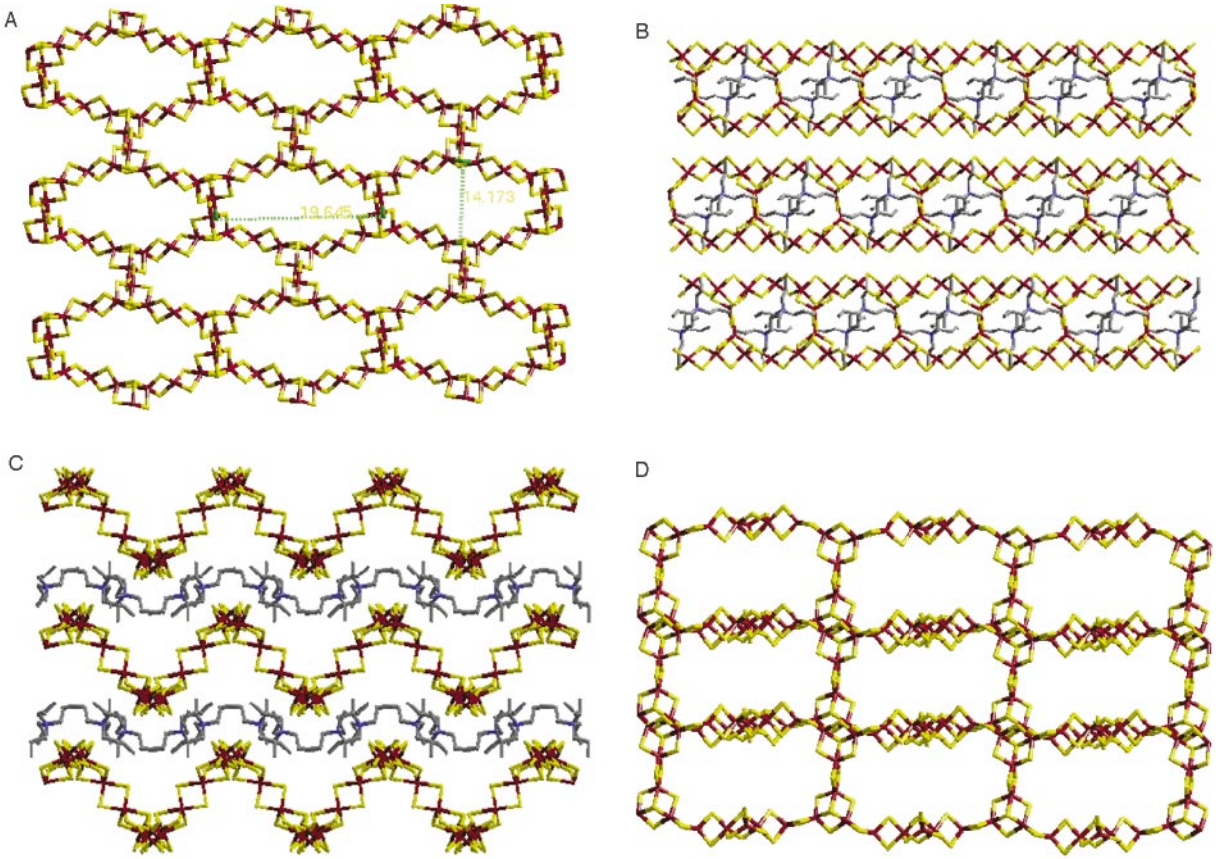

Fig. 5 Illustrations of the structure of TPA-SnS-3 (color notation: dark red, Sn; yellow, S; blue, N; grey, C). (A) Projection of the [−101] plane with the template cations omitted for clarity [note the elliptical 32-atom rings built-up of Sn_3S_7 broken-cube clusters which are linked together by tetrahedral edge-bridging $Sn(\mu\text{-}S_2SnS_2)Sn$ spacer units as well as double sulfide $Sn(\mu\text{-}S)_2Sn$ bridge bonds], (B) projection of the [101] plane including the template cations TPA^+ that are located between the layers (note the corrugated architecture of both the tin sulfide framework and the imbibed TPA^+ template), (C) projection of the [010] plane including the template ions that are located within the layers (note that the corrugated nature of the TPA-SnS-3 layers creates the illusion of 20-atom rings when the structure is viewed in this direction), (D) projection of the [−111] plane with the template cations omitted for clarity (note that as described in the text, the corrugated layers can be viewed as a staircase and when viewed normally to the steps, the elliptical-shaped 32-atom rings become pseudo-rectangular).

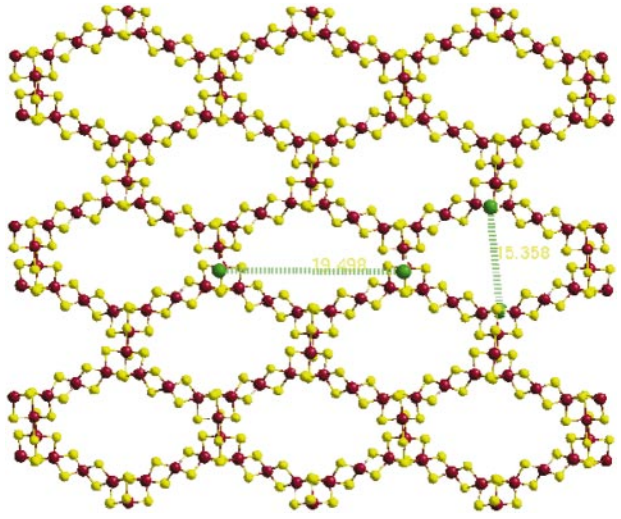

Fig. 6 Illustration of the structure of TBA-SnS-3 (color notation: dark red, Sn; yellow, S; blue, N; grey, C). Projection of the [001] plane with the template cations omitted for clarity. Note that the overall structure of the open-framework of TBA-SnS-3 is the same as that of TPA-SnS-3; however, the size and shape of the elliptical-shaped 32-atom rings are different.

samples for property measurements. However, the PXRD pattern of the products always displayed additional peaks besides those calculated for the original TPA-SnS-3 phase (based on the single crystal structure data). It seemed impossible to synthesize a phase-pure TPA-SnS-3 material until it was discovered that the intensity of the extra peaks was related to the crystal size of the products; the larger the crystals, the stronger the additional peaks. Large single crystals of TPA-SnS-3, that were structurally characterized by SCXRD analysis, surprisingly gave rise to the cleanest PXRD pattern of TPA-SnS-3(II) if care was not taken with the grinding procedure. However, with gentle grinding of the same crystals, a nearly phase-pure TPA-SnS-3 powder XRD pattern resulted. Small crystals of a few μm in size, that do not require much grinding for powder XRD data collection, indeed yielded a pure TPA-SnS-3 PXRD pattern. It should be mentioned that single crystals of TPA-SnS-3 tend to display different colors from light yellow to orange–red; in addition, aggregates of crystals exhibit many shapes. Therefore at the early stages of this study, it was not clear whether the TPA-SnS-3 single crystal structure was representative of the whole crop of crystals. This was later confirmed by a PXRD study. The colors displayed by the TPA-SnS-3 crystals are believed to originate from defects in the structure. For example, if some Sn^{IV} sites are by chance replaced by Sn^{II}, additional electronic states would be introduced in the band-gap below the conduction band of the TPA-SnS-3 structure; thus absorption of visible light with energy lower than the band-gap becomes possible. Another possibility is that some sulfur vacancies in the framework arising from non-stoichiometry in the number of charge-balancing templates could also create some defect states in the band-gap and above the valence band which could also give rise to color. Pure TPA-SnS-3 powders are off-white.

Table 6 A summary of the dimensions of the 24-atom rings and the interlayer spacing and layer stacking sequences of various SnS-1 materials

R-SnS-1 material	pore dimensions[a]/ Å × Å × Å	interlamellar spacing/Å	stacking sequence	space group
$Cs_2Sn_3S_7 \cdot 1/2S_8$	10.79 × 10.79 × 10.47	8.151	AB	$C2/c$
$(Me_4N)_2Sn_3S_7 \cdot H_2O$	11.69 × 11.03 × 9.69	8.511	AA	$P2_1/n$
$(DABCOH)_2Sn_3S_7 \cdot H_2O$	10.98 × 10.98 × 9.95	8.594	AB	$C2/c$
$(NH_4)_{0.5}(Et_4N)_{1.5}Sn_3S_7$	10.94 × 10.94 × 10.88	9.011	ABC	$P3_121$
$(Et_4N)_2Sn_3S_7$	11.58 × 10.84 × 10.42	8.915	AA	$P2_1/n$

[a]Dimensions defined from sulfur center to sulfur center as illustrated in Fig. 3A.

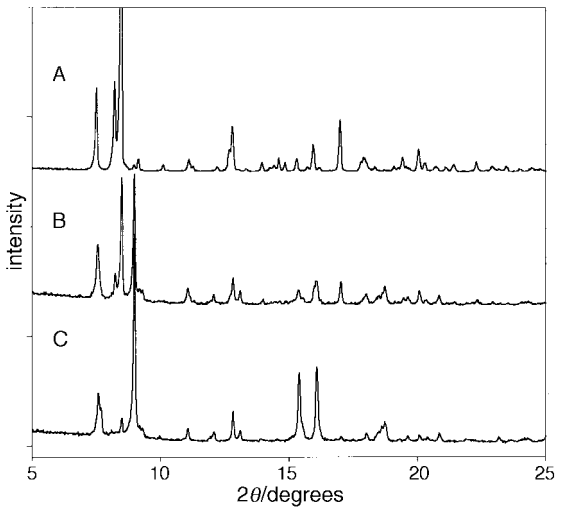

Fig. 7 PXRD patterns of TPA-SnS-3 (A) as-synthesized, (B) after being ground manually in a mortar, and (C) further ground (B)

Analysis of the phase-pure powder form of R-SnS-*n* materials

Powder X-ray diffraction patterns (PXRD) and elemental analysis

The PXRD patterns of the SnS-*n* materials are shown in Fig. 8, together with the simulations calculated from the single crystal structure data. The excellent match of the experimental patterns with the simulations indicates that highly crystalline SnS-*n* samples were successfully produced that do not contain any form of crystalline impurities.[14] Mössbauer and Raman spectra of these materials have further confirmed the absence of amorphous impurities in these samples.[11*b*] Elemental analysis results of the SnS-*n* materials are summarized in Table 7. They agree well with the calculated values based on the formulae established by the single crystal XRD analysis. The exception is the TEA-SnS-1 sample, in which the content of Et_4N^+ is found to be *ca.* 10% less than the calculated value. This is believed to originate from partial decomposition of Et_4N^+ to smaller amines during the hydrothermal crystallization process. It has been reported by Parise *et al.* that Me_4N^+ partially decomposes to Me_3NH^+ during the crystallization of TMA-SnS-1 under similar reaction conditions to those used in this work.[17] *In situ* pressure measurements during the crystallization of the SnS-*n* materials have also been conducted in this laboratory. The TEA-SnS-1 system was found to have the highest pressure in comparison with TMA-SnS-1 and TPA-SnS-3 when starting with the same reaction mixture stoichiometry under identical crystallization conditions. The higher pressure observed in the TEA-SnS-1 system is presumably due to the decomposition of Et_4N^+ to smaller organics, like Et_3N, EtSH and Et_2S. This would have increased the total number of molecules in the reactor and thus the total pressure. Smaller amines formed in this way may have also been incorporated into the final TEA-SnS-1 structure as co-templating agents. The presence of organics other than Et_4N^+ in the final product structure is believed to be partly responsible for the difficulty experienced in the elemental analysis and locating the other Et_4N^+ template in the TEA-SnS-1 structure by SCXRD analysis. The extreme sensitivity of the TEA-SnS-1 unit cell and structure to small adsorbed guest molecules might be another cause. It was found that a dehydrated TEA-SnS-1 sample experiences a unit cell volume expansion of almost 6% and a decrease of the monoclinic angle β from 95.3 to 90.1° when exposed to water vapor at room temperature.[20]

Effect of crystallization conditions on the product phase identity

Agitation

It should be mentioned that the microporous layered SnS-*n* materials are topologically metastable phases. They are kinetic, instead of thermodynamic products. In general, in the synthesis of microporous metastable materials, a phase which is most energetically favorable will form first, and successively transform, *via* for example Ostwald ripening, to more thermodynamically favorable phases with reaction time.[22] A change in reaction profile, such as time, temperature, aging and agitation, may completely alter the phase identity of the final product. As a result, the synthesis of phase-pure SnS-*n* materials sometimes is not as straightforward as one would have anticipated. It was discovered in the course of this work that some phases can only be produced under static crystallization conditions. For example, a highly crystalline TEA-SnS-1 sample was formed under static reaction conditions, from a reaction mixture of $TEAOH : 23\,H_2O : Sn : 2\,S$ at 150 °C for 3 days. However, a new phase, denoted TEA-SnS-2, resulted from the same reaction mixture, temperature and time, upon crystallization under dynamic conditions in a tumbler reactor. Agitation has completely altered the phase identity of the final product! Recall that both Me_4N^+ and Et_4N^+ directed the formation of the SnS-1 structure type, while $Pr^n{}_4N^+$ and $Bu^n{}_4N^+$ directed the SnS-3 structure type. Actually, Et_4N^+ is the largest template reported to direct the formation of the SnS-1 structure type. When a mixture of Et_4N^+ and $Pr^n{}_4N^+$ was used as a templating agent, a new product was formed, the PXRD pattern of which does not resemble any of the known SnS-1 family. It appears that the size of the Et_4N^+ cation might be the upper limit for templating SnS-1 type structures. Templates larger than Et_4N^+ yield materials with pores larger than the 24-atom ring present in the SnS-1 structure. The relatively large size of Et_4N^+ with respect to the void space in the SnS-1 structure type may provide many free energy minima involving different arrangements of the tin sulfide framework and tetraethylammonium cations. It is also known in the zeolite literature that Et_4N^+ can exist as different conformational isomers with similar energy. Therefore, depending on the crystallization conditions, many SnS-*n* structure types can be formed from the tetraethylammonium system. As TEA-SnS-2 has so far only formed under dynamic reaction conditions, sufficiently large single crystals could not be obtained for SCXRD structure analysis.

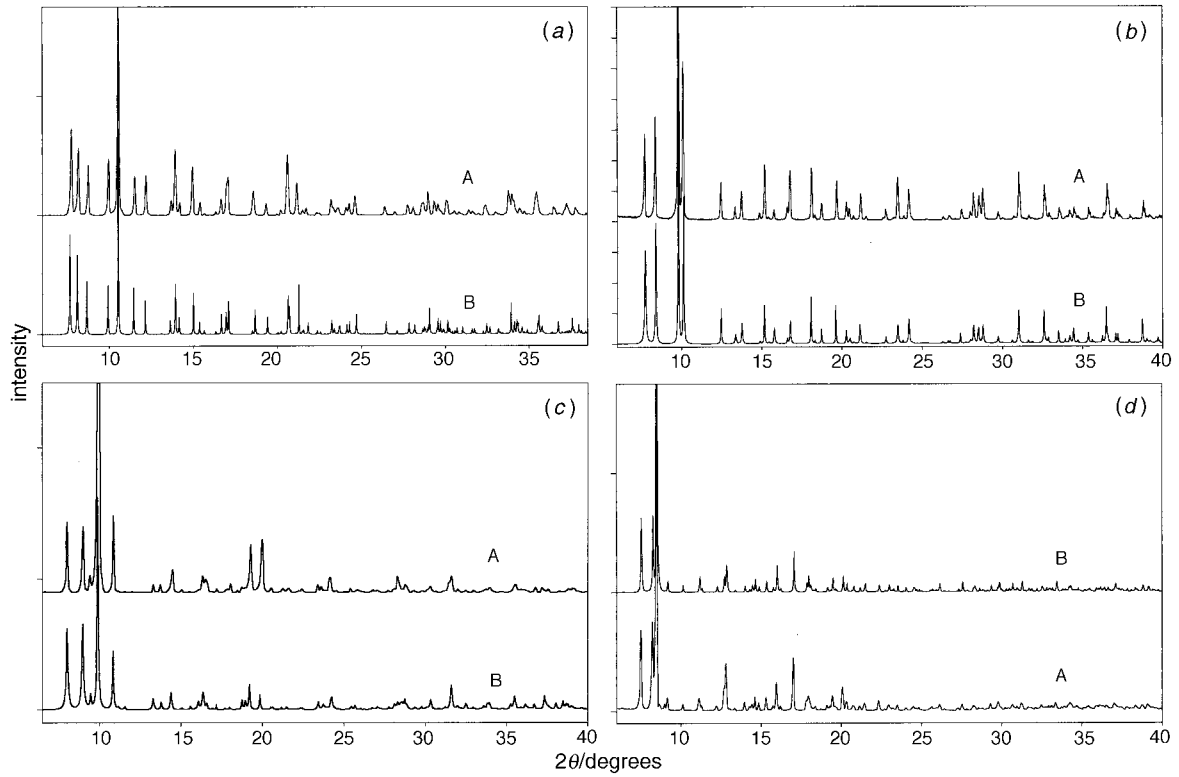

Fig. 8 Experimental (A) and calculated (B) PXRD patterns of (*a*) DABCOH-SnS-1, (*b*) ATEA-SnS-1, (*c*) TEA-SnS-1 and (*d*) TPA-SnS-3

Table 7 A summary of the elemental analysis results of the phase-pure SnS-*n* materials

R-SnS-*n* material		Sn	S	C	N	H	H_2O
$(NH_4)_{0.5}(Et_4N)_{1.5}Sn_3S_7{\cdot}(H_2O)_3$	calc.	42.46	26.76	17.17	3.33	3.85	6.45
(ATEA-SnS-1)	found	42.63	26.57	17.20	3.23	3.80	6.47
$(Et_4N)_2Sn_3S_7{\cdot}(H_2O)_2$	calc.	40.65	25.57	21.92	3.20	4.57	4.10
(TEA-SnS-1)	found	41.72	26.66	19.61	3.12	4.14	4.72
$(DABCOH)_2Sn_3S_7{\cdot}(H_2O)_3$	calc.	41.31	26.04	16.71	6.50	3.02	6.90
(DABCOH-SnS-1)	found	41.55	26.04	16.45	6.46	2.95	6.53
$(Pr^n{}_4N)_2Sn_4S_9{\cdot}H_2O$	calc.	41.18	24.98	24.98	2.43	4.86	1.56
(TPA-SnS-3)	found	40.92	25.28	24.59	2.29	4.89	1.53

Aging

The effect of aging on the phase identity of final products has also been investigated. Starting from an identical reaction mixture of TPAOH : 84 H_2O : Sn : 2 S, a static crystallization at 150 °C for 3 days, without aging at room temperature, has resulted in highly crystalline TPA-SnS-3 samples, whereas aging at room temperature for 7 days before heating at 150 °C, has resulted in a new phase, denoted TPA-SnS-4. Interestingly, TPA-SnS-4 has also been crystallized from TPAOH : 84 H_2O : SnS_2 statically at 150 °C for 3 days. A change of tin and sulfur source materials from the elements to tin disulfide has also caused the formation of new phases.

Crystallization time

The effect of reaction time on the phase identity of final products has also been the subject of study. A reaction mixture of TEAOH : $(NH_4)_2S$: 30 H_2O : Sn : 2 S, crystallized at 150 °C for 3 days, resulted in pure ATEA-SnS-1 materials; however, TEA-SnS-1 clearly was simultaneously formed over a period of 14 days. It was also found that starting from the same reaction mixture, an increase of crystallization temperature to 180 °C favors the formation of the TEA-SnS-1 phase. This implies that the TEA-SnS-1 structure is more thermodynamically stable than the ATEA-SnS-1. This may be attributed to the higher packing density and therefore higher stability of TEA-SnS-1, in comparison with ATEA-SnS-1 (Tables 3 and 4).

Conclusions

The synthesis and structure of several SnS-*n* materials have been studied. Synthetic routes have been developed that yield large single crystals and phase-pure SnS-*n* materials. The microporous layered structures of two types of tin sulfide-based materials, SnS-1 and SnS-3, have been established through single crystal XRD analysis. Elemental analysis of phase-pure materials is found to be in good agreement with the formulae determined by single crystal XRD structure analysis, $A_2Sn_3S_7$ for the SnS-1 and $A_2Sn_4S_9$ for the SnS-3 structure type. Templating effects were observed in the synthesis of these materials, *i.e.* larger template molecules result in larger void spaces within and between the tin sulfide sheets. Unique framework flexibility was discovered for both structure types. In order to accommodate the size/shape changes of templates, the microporous tin(IV) sulfides are able to undergo a certain degree of elastic deformation to alter the void spaces within and between the porous layers, rather than forming a completely new porous structure type. This may explain the relatively small number of tin sulfide-based structure types

discovered so far, in comparison with the diversity of oxide-based open-framework structures. Although the three reported SnS-1 materials have similar framework topology, owing to the different size and locations of templates in the structure, these materials have different porosity and display distinct guest-molecule adsorption behavior.[11b] For example, the 24-atom ring in a dehydrated DABCOH-SnS-1 sample is empty, and consequently this material displays a type 1 adsorption isotherm towards small guest molecules, such as CO_2 and H_2O. However, the 24-atom rings in dehydrated TEA-SnS-1 and ATEA-SnS-1 samples are partially occupied by the hydrocarbon arms of Et_4N^+ cations, and as a result they discriminate CO_2 and selectively adsorb H_2O. The adsorption of water in these two materials is found to be an integration of void-filling and intercalation, and displays a type 2 adsorption isotherm. Detailed adsorption and chemical sensing results will be published in a separate paper. The TPA-SnS-3 framework is also found to be pressure sensitive, and readily transforms to TPA-SnS-3(II) by moderate, manual grinding of the material in a mortar.

The formation of metastable SnS-*n* materials was found to be very sensitive to the choice of source materials and the composition of reaction mixtures, as well as crystallization conditions such as time, temperature, agitation and aging. This makes the synthesis of a particular SnS-*n* material, in both large single crystal and phase-pure powder forms, a challenging task. In general, static crystallization conditions favor the growth of large single crystals, however, accompanied by a significant amount of unreacted tin metal. On the other hand, dynamic crystallization in a tumbling reactor favors the formation of phase-pure materials of small crystal size, most often around a couple of μm.

Experimental

Reagents

Tin metal (99.8%, 325 mesh), sulfur powder (sublimed, 100 mesh), Et_4NOH (35% aqueous solution), $Pr^n{}_4NOH$ (1 M aqueous solution), $Bu^n{}_4NOH$ (40% aqueous solution), $(NH_4)_2S$ (20% aqueous solution), NH_4F (97%) purchased from Aldrich; 1,8-diazabicyclooctane (97%) from Fluka were used directly for synthesis without further purification.

Synthesis

The optimised reaction mixtures for the synthesis of the SnS-*n* materials are listed in Tables 1 and 2. The general procedure is to first dissolve the alkylammonium hydroxide, amine, $(NH_4)_2S$ and NH_4F in deionized water, followed by addition of sulfur and tin powders. The mixture was stirred at room temperature for 20 min, then sealed in a Teflon-lined stainless steel reactor, following the temperature treatment described in Tables 1 and 2. The product was recovered by filtration and washed with copious amounts of water and acetone, then dried in air. [*Note* that the handling of the SnS-*n* materials must be conducted in a fume hood and great care must be taken with the storage and disposal of toxic waste.]

Physical measurements

Powder X-ray diffraction patterns were collected on a Siemens D-5000 diffractometer with Cu-Kα radiation. A summary of crystallographic and structure refinement data is given in Tables 3 and 4. For DABCOH-SnS-1, data were collected on a Siemens P4 diffractometer using graphite-monochromated Mo-Kα radiation ($\lambda = 0.71073$ Å). The intensities of three standard reflections measured every 97 reflections showed no decay. The data were corrected for Lorentz and polarization effects and an absorption correction was applied using psi-scan data. Minimum and maximum absorption corrections were 0.2703 and 0.7661. The structure was solved and refined using the SHELXTL`PC package.[23] Refinement was performed using full-matrix least-squares on F^2 using all data (negative intensities included). The weighting scheme was $w = 1/[\sigma^2(F_o{}^2) + (0.0463P)^2]$ where $P = (F_o{}^2 + 2F_c{}^2)/3$. All hydrogen atoms were included in calculated positions (and treated as riding atoms) except for the NH hydrogens which were refined with isotropic thermal parameters. The hydrogen atoms from the water molecule of solvation were not included in the refinement. For TEA-SnS-1 data were collected on an Enraf-Nonius CAD4 diffractometer using graphite-monochromated Mo-Kα radiation ($\lambda = 0.71073$ Å). Good single crystals of TEA-SnS-1 were difficult to select. Larger crystals appeared to be aggregates of very thin plates. The crystal selected for data collection was the smallest fragment possible (for a single crystal experiment of this type) cut from the edge of a larger crystal. We were able to determine an orientation matrix and unit cell with the aid of the DIRAX program.[24] The intensities of three standard reflections measured every 2 h showed no decay. The data were corrected for Lorentz and polarization effects and an absorption correction was applied using psi-scans. Minimum and maximum absorption corrections were 0.2610 and 0.9730. The structure was solved and refined using the SHELXTL`PC package.[23] Refinement was by full-matrix least-squares on F using data which had $F > 6\sigma(F)$. The weighting scheme was $w = 1/\sigma^2(F_o{}^2) + 0.0135F^2$. Sn and S atoms were refined with anisotropic thermal parameters and C and N atoms were refined with isotropic thermal parameters. Not all of the atoms of the template molecules were located. It was suspected that some of the template molecules which lie in between the $[Sn_3S_7]^{2-}$ layers were disordered over several crystallographic sites and some may have transformed to smaller organic molecules during the crystallization process. The data for ATEA-SnS-1 were collected on a Siemens SMART system at the University of Illinois at Urbana-Champaign by Dr. Scott Wilson. The refinement procedure used was similar to that used for DABCOH-SnS-1.

The financial assistance of the Natural Sciences and Engineering Research Council of Canada (NSERC), the Canadian Space Agency (CSA) and Universal Oil Products (UOP) is deeply appreciated. Insightful discussions with Dr. Srebri Petrov about powder X-ray diffraction analysis have proven to be invaluable. Technical assistance from Dr. Neil Coombs in obtaining the SEM images is deeply appreciated. The assistance of Dr. Walter Zamachek with elemental analysis is gratefully acknowledged. We are also grateful to Dr. Scott Wilson at the University of Illinois at Urbana-Champaign for collecting the single crystal diffraction data of ATEA-SnS-1.

References

1 (*a*) D. W. Breck, *Zeolite Molecular Sieves: Structure, Chemistry and Use*, Wiley and Sons, London, 1974; (*b*) S. M. Csicsery, *Chem. Br.*, 1985, **21**, 473; (*c*) G. A. Ozin, *Adv. Mater.*, 1992, **4**, 612.
2 (*a*) W. S. Sheldrick and M. Wachhold, *Angew. Chem., Int. Ed. Engl.*, 1997, **36**, 206; (*b*) C. L. Bowes and G. A. Ozin, *Adv. Mater.*, 1996, **8**, 13; (*c*) M. G. Kanatzidis, *Chem. Mater.*, 1990, **2**, 353.
3 (*a*) R. L. Bedard, L. D. Vail, S. T. Wilson and E. M. Flanigen, *US Pat.*, 1989, 4 800 761; (*b*) R. L. Bedard, L. D. Vail, S. T. Wilson and E. M. Flanigen, *US Pat.*, 1990, 4 933 068; (*c*) R. L. Bedard, S. T. Wilson, L. D. Vail, J. M. Bennett and E. M. Flanigen, in *Zeolites: Facts, Figures, Future*, ed. P. A. Jacobs and R. A. van Santen, *Stud. Surf. Sci. Catal.*, vol. 49, part A, Elsevier Science Publishers B.V., Amsterdam, 1989.
4 (*a*) G. A. Ozin, in *Materials Chemistry, an Emerging Subdiscipline, ACS Symp., Washington, 1992*, ed. L. Interrante, *Adv. Chem. Ser.*, ACS, Washington, DC, 1995, **245**, 335; (*b*) M. A. Reed, *Sci. Am.*, 1993, 118; (*c*) R. L. Bedard, G. A. Ozin, H. Ahari, C. L. Bower and D. Young, *US Pat.*, 1997, 5 594 263.
5 J. B. Parise, Y. Ko, J. Rijssenbeek, D. M. Nellis, K. Tan and S. Koch, *J. Chem. Soc., Chem. Commun.*, 1994, 527.
6 G. A. Marking and M. G. Kanatzidis, *Chem. Mater.*, 1995, **7**, 1915.

7 T. Jiang, A. J. Lough, G. A. Ozin, R. L. Bedard and D. Young, *Chem. Mater*., 1995, **7**, 245.
8 (*a*) J. J. Mullin, *Crystallization*, Butterworths, London, 1961; (*b*) I. V. Markov, *Crystal Growth for Beginners*, World Scientific, New Jersey, 1995; (*c*) R. A. Laudise, *The Growth of Single Crystals*, Prentice-Hall, New Jersey, 1970.
9 R. M. Barrer, in *Zeolite Synthesis*, ed. M. L. Occelli and H. E. Robson, ACS Symposium Ser. 398, American Chemical Society, Washington, DC, 1989.
10 P. A. Jacobs, in *Zeolite Microporous Solids; Synthesis, Structure and Reactivity*, ed. E. G. Derouane, F. Lemos, C. Naccache and F. R. Ribeiro, NATO ASI Series, Ser. C, vol. 352, Kluwer Academic Publishers, Dordrecht, 1992.
11 (*a*) T. Jiang and G. A. Ozin, *Adv. Mater*., in press; (*b*) T. Jiang, PhD Thesis, University of Toronto, 1997; (*c*) T. Jiang, G. A. Ozin and R. L. Bedard, *Adv. Mater*., 1994, **6**, 860.
12 J. Robertson, *J. Phys. C: Solid State Phys*., 1979, **12**, 4753.
13 J. E. Huheey, *Inorganic Chemistry: Principles of Structure and Reactivity*, Harper & Row, New York, 1983, ch. 6.
14 With respect to the high R values for the TEA-SnS-1 SC XRD structure refinement, and the goodness-of-fit between the observed and simulated PXRD patterns of the material. In this particular structure determination the origin of the high wR_2 most likely arises from the fact that the crystals were of fairly poor quality; that is, a weak diffractor and of high mosaicity. The weak reflections which were measured with high statistical error were rejected from the least-squares refinement but were included in the final calculation of wR_2. Furthermore, one of the templates in the structure is disordered and there is expected to be some contribution in the framework from fragmentation of the tetraethylammonium template in a 150 °C hydrothermal synthesis. The refinement is, however, quite sufficient to discuss the overall framework structure of the microporous layered tin sulfide but not the details of their bond lengths and angles. It should be mentioned that considering neither charge-balancing tetraethylammonium template cations nor physisorbed/chemisorbed water guests were included in the calculation of the PXRD pattern of the TEA-SnS-1 structure, the goodness-of-fit between the observed and simulated patterns is remarkably good, and within the limits of the model presented quite acceptable for the purpose used in this study.
15 (*a*) R. Szostak, *Molecular Sieves: Principles of Synthesis and Identification*, Van Nostrand Reinhold, New York, 1989, ch. 2; (*b*) R. M. Barrer, *Hydrothermal Chemistry of Zeolites*, Academic Press, London, 1982; (*c*) *Zeolite Synthesis*, ed. M. L. Occelli and H. E. Robson, ACS Symposium Series 398, American Chemical Society, Washington DC, 1989; (*d*) M. E. Davis, *Chem. Mater*., 1992, **4**, 756; (*e*) M. E. Davis, *Acc. Chem. Res*., 1993, **26**, 111.
16 (*a*) C. T. Kresge, M. E. Leonowicz, W. J. Roth, J. C. Vartuli and J. C. Beck, *Nature* (*London*), 1992, **359**, 710; (*b*) S. Mann and G. A. Ozin, *Nature* (*London*), 1996, **382**, 313.
17 K. Tan, Y. Ko and J. B. Parise, *Acta Crystallogr., Sect. C*, 1995, **51**, 398.
18 W. S. Sheldrick, *Z. Anorg. Allg. Chem*., 1988, **562**, 23.
19 (*a*) D. R. Corbin, L. Abrams, G. A. Johns, M. M. Eddy, W. T. A. Harrison, G. D. Stucky and D. E. Cox, *J. Am. Chem. Soc*., 1990, **112**, 4821; (*b*) C. A. Fyfe, H. Strobl, G. Kokotailo, G. J. Kennedy and G. E. Barlow, *J. Am. Chem. Soc*., 1988, **110**, 3373.
20 (*a*) H. Ahari, C. L. Bowes, T. Jiang, A. Lough, G. A. Ozin, R. L. Bedard, S. Petrov and D. Young, *Adv. Mater*., 1995, **7**, 375; (*b*) G. A. Ozin, *Supramol. Chem*., 1995, **6**, 125; (*c*) G. A. Ozin, C. L. Bowes, T. Jiang, A. Lough, S. Petrov, G. Vouk, A. Verma and D. Young, *Electrical Sieves for Molecular Recognition*, in *Molecular Recognition and Inclusion*, ed. A. Coleman, Kluwer Academic, Dordrecht, The Netherlands, 1997.
21 (*a*) B. Palosz, W. Steurer and H. Schulz, *Acta Crystallogr., Sect. B*, 1990, **46**, 449; (*b*) B. Palosz, W. Palosz and S. Gierlotka, *Acta Crystallogr., Sect. C*, 1986, **42**, 653; (*c*) A. R. Verma and P. Krishna, *Polymorphism and Polytypism in Crystals*, John Wiley & Sons, New York, 1969.
22 J. Gopalakrishanan, *Chem. Mater*., 1995, **7**, 1267.
23 G. M. Sheldrick, SHELXTL`PC, Siemens Analytical X-ray Instruments Inc., Madison, Wisconsin, 1994.
24 A. J. M. Duisenberg, *J. Appl. Crystallogr*., 1992, **25**, 92.

Paper 7/06279F; *Received* 27*th August*, 1997